SIAM J. NUMER. ANAL.
Vol. 45, No. 4, pp. 1425–1452

CONVERGENCE OF A NUMERICAL METHOD FOR SOLVING DISCONTINUOUS FOKKER–PLANCK EQUATIONS*

HONGYUN WANG†

Abstract. In studies of molecular motors, the stochastic motion is modeled using the Langevin equation. If we consider an ensemble of motors, the probability density is governed by the corresponding Fokker–Planck equation. Average quantities, such as average velocity, effective diffusion coefficient, and randomness parameter, can be calculated from the probability density. A numerical method was previously developed to solve Fokker–Planck equations [H. Wang, C. Peskin, and T. Elston, *J. Theoret. Biol.*, 221 (2003), pp. 491–511]. It preserves detailed balance, which ensures that if the system is forced to an equilibrium, the numerical solution will be the same as the Boltzmann distribution. Here we study the convergence of this numerical method when the potential has a finite number of discontinuities at half numerical grid points. We prove that this numerical method is stable and is consistent with the differential equation. Based on the consistency analysis, we propose a modified version of this numerical method to eliminate the first order error term caused by the discontinuity. We also show that in the presence of discontinuities, detailed balance is a necessary condition for converging to the correct solution. This explains why the central difference method converges to a wrong solution.

Key words. Fokker–Planck equation, detailed balance, consistency, stability, convergence

AMS subject classification. 65M

DOI. 10.1137/050639442

1. Introduction.

Molecular motors operate in an environment dominated by thermal fluctuations [1]. In general, a molecular motor has many internal and external degrees of freedom. Of these degrees of freedom, there is one associated with the main function of the motor, its unidirectional motion. For example, the γ shaft of an F_1 ATPase rotates with respect to the hexamer formed by three pairs of α and β subunits [2, 3, 4], and a kinesin dimer walks along a microtubule [5, 6]. In studies of molecular motors, it is natural to follow the motor along the dimension of its unidirectional motion [7, 8, 9]. The effects of the other degrees of freedom are modeled in the mean field potential affecting the unidirectional motion.

To introduce the governing equations for molecular motors, we start with the one-dimensional motion of a small particle in a fluid environment subject to a potential, $V(x)$, where x is the coordinate along the dimension of motion. The particle is subject to the viscous drag force, the force derived from the potential, and the Brownian force. Both the drag force and the Brownian force are the results of bombardments by surrounding fluid molecules. The drag force is the mean, and the Brownian force is the fluctuation part of the random force caused by bombardments. The particle is governed by Newton's second law:

$$m\frac{dv}{dt} = -\zeta v - V'(x) + \sqrt{2k_BT\zeta}\,\frac{dW(t)}{dt}, \tag{1.1}$$

where m is the mass and v the velocity of the particle. In (1.1), $W(t)$ is the Weiner process. The drag force on the particle, ζv, is proportional to the velocity, and ζ is

*Received by the editors September 2, 2005; accepted for publication (in revised form) January 16, 2007; published electronically July 18, 2007. This work was partially supported by National Science Foundation grant DMS-0317937.

http://www.siam.org/journals/sinum/45-4/63944.html

†Department of Applied Mathematics and Statistics, Mail Stop SOE2, University of California Santa Cruz, Santa Cruz, CA 95064 (hongwang@ams.ucsc.edu).

called the drag coefficient. The magnitude of the Brownian force is related to the drag coefficient and is given by $\sqrt{2k_BT\zeta}$, which is a result of the fluctuation-dissipation theorem [11, 13]. Here k_B is the Boltzmann constant and T the absolute temperature.

For a bead of radius a, the drag coefficient and the mass, respectively, are [1]

$$\zeta = 6\pi\eta a, \qquad m = \frac{4}{3}\pi\rho a^3, \tag{1.2}$$

where ρ is the density and η the viscosity of the surrounding fluid. Equation (1.1) can be written as

$$\frac{dv}{dt} = -\frac{\zeta}{m}\left(v - \left[-\frac{1}{\zeta}V'(x) + \sqrt{2D}\frac{dW(t)}{dt}\right]\right), \tag{1.3}$$

where $D = \frac{k_BT}{\zeta}$ is the diffusion constant [1]. It is important to notice that the ratio $\frac{\zeta}{m}$ is inversely proportional to the square of the radius of particle

$$\frac{\zeta}{m} = \frac{9\eta}{2\rho a^2} = O\left(\frac{1}{a^2}\right). \tag{1.4}$$

Thus, for a small particle, $\frac{\zeta}{m}$ is very large. In this case, (1.3) is well approximated by

$$v = \left[-\frac{1}{\zeta}V'(x) + \sqrt{2D}\frac{dW(t)}{dt}\right]. \tag{1.5}$$

The reduction from (1.3) to (1.5) in the limit of large $\frac{\zeta}{m}$ is called the Kramers–Smoluchowski approximation. Writing (1.5) as a stochastic differential equation for x, we have

$$\frac{dx}{dt} = -\frac{1}{\zeta}V'(x) + \sqrt{2D}\frac{dW(t)}{dt}. \tag{1.6}$$

This is the Langevin equation without the inertia term, governing the stochastic motion of a small particle subject to potential $V(x)$ [12].

In molecular motors, the mechanical motion is coupled to the chemical reaction. The general mathematical framework used in modeling molecular motors is a system of coupled Langevin equations. Each Langevin equation in the coupled system has the form of (1.6) with a periodic potential $V_S(x)$, where S represents the current chemical state of the motor system [7, 9, 4]:

$$\frac{dx}{dt} = -\frac{1}{\zeta}V_S'(x) + \sqrt{2D}\frac{dW(t)}{dt}. \tag{1.7}$$

Here $1 \le S \le N$, and N is the number of possible chemical states of the motor system. The period of these potentials is usually determined by the step size of the motor. For example, a kinesin dimer walks on a microtubule with 8-nm steps [6]. The chemical reaction of the motor system (the stochastic jumping of the motor system among the chemical states) is governed by a discrete Markov process (a jump process).

The motor behavior (such as the average velocity) can be calculated by following the stochastic evolution (mechanical motion and chemical reaction) of the motor in Monte Carlo simulations. However, results obtained with Monte Carlo simulations have statistical errors and converge very slowly. If we calculate the ensemble average

by following a large number of motors, then the statistical error is inversely proportional to the square root of the number of motors in the ensemble. Furthermore, when the potential $\psi(x)$ is not smooth, there are numerical difficulties in Monte Carlo simulations. Fortunately, average quantities can be calculated more efficiently by following the probability density of the motor.

Let us consider an ensemble of motors, each evolving in time independently and stochastically according to Langevin equation (1.7). Let $\rho_S(x,t)$ be the probability density that the motor is at position x and in chemical state S at time t. The time evolution of $\rho_S(x,t)$ is governed by the Fokker–Planck equation corresponding to Langevin equation (1.7) [12]:

$$\frac{\partial \rho_S}{\partial t} = D\frac{\partial}{\partial x}\left[\frac{V_S'(x)}{k_BT}\rho_S + \frac{\partial \rho_S}{\partial x}\right] + \sum_{j=1}^{N} k_{j\to S}(x)\rho_j, \qquad S = 1, 2, \ldots, N, \tag{1.8}$$

where, for $j \neq S$, $k_{j\to S}(x)$ is the chemical transition rate from state j to state S. $k_{S\to S}(x)$ is the total rate of jumping out of state S and is given by

$$k_{S\to S}(x) \equiv -\sum_{j\neq S} k_{S\to j}(x). \tag{1.9}$$

A simple way to model molecular motors is to average $V_S'(x)$ over all chemical states weighted by the steady state probability density functions of these states [10]. Let $\psi'(x)$ be the weighted average of $V_S'(x)$ over all chemical states:

$$\psi'(x) \equiv \frac{1}{\sum_{S=1}^{N}\rho_S(x)}\sum_{S=1}^{N}\rho_S(x)V_S'(x). \tag{1.10}$$

$\psi(x)$ can be viewed as the motor's mean field free energy landscape. The mechanical motion of the motor can be modeled using Langevin equation (1.6) with potential $\psi(x)$. Let L denote the period of $V_S(x)$. We immediately see that $\psi'(x)$ is also periodic with period L. However, $\psi(x)$ may not be periodic. As a matter of fact, for a molecular motor undergoing a unidirectional motion powered by a chemical reaction, $\psi(x)$ must not be periodic. If $\psi(x)$ is periodic, then there is no energy available to drive the motor forward because there is no free energy change going from one period to the next. For the motor to go forward, there must be a free energy drop going from one period to the next. Since $\psi'(x)$ is periodic, the energy landscape $\psi(x)$ is a tilted periodic potential:

$$\psi(x+L) = \psi(x) - \Delta\psi, \tag{1.11}$$

where $\Delta\psi > 0$ is the energy made available from the chemical reaction to drive the motor forward in one period. An example of tilted periodic potential is shown in Figure 1.1. This is also the potential we will use in numerical simulations in section 7. If the energy landscape $\psi(x)$ is simply a constant slope downhill, then the energy $\Delta\psi$ is utilized uniformly in one period to generate a constant motor force. If the slope of $\psi(x)$ is not a constant, then the motor force varies with the motor position within one period. As shown in Figure 1.1, the energy landscape $\psi(x)$ may not be monotonic. In that case, the motor depends on the Brownian fluctuations from the surrounding fluid to get over the free energy barrier. Of course, the energy source for driving the motor forward eventually comes from the free energy drop $\Delta\psi$, which rectifies

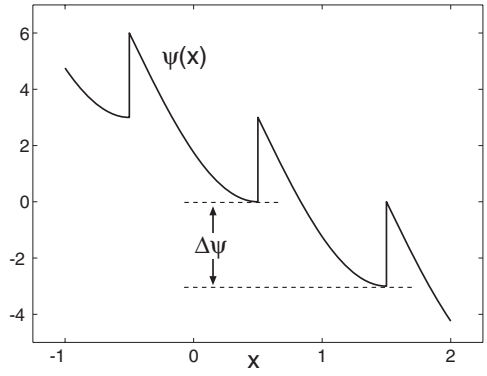

FIG. 1.1. *Graph of the tilted periodic potential used in numerical simulations in section 7.*

the forward fluctuations. This mechanism of driving the motor forward by rectifying thermal fluctuations is called ratchet [22].

If we use the mean field potential (1.10), then the mechanical motion of the motor is governed by the Langevin equation:

$$\frac{dx}{dt} = -\frac{1}{\zeta}\psi'(x) + \sqrt{2D}\frac{dW(t)}{dt}. \tag{1.12}$$

Equation (1.12) has been used in studies of motors [14, 15]. In addition to its mathematical simplicity, another advantage of using (1.12) is that the energy landscape $\psi(x)$ can be extracted from single molecule experimental data [10]. The Fokker–Planck equation corresponding to Langevin equation (1.12) is [12]

$$\frac{\partial \rho}{\partial t} = D\frac{\partial}{\partial x}\left[\frac{\psi'(x)}{k_B T}\rho + \frac{\partial \rho}{\partial x}\right]. \tag{1.13}$$

In [16], a robust numerical method (hereafter referred to as Method 1) was designed for solving Fokker–Planck equations (1.8) and (1.13). When the potential is smooth, the proof of convergence of Method 1 is straightforward [16]. But that does not provide an accurate theoretical explanation for the robust performance of Method 1. The strength of Method 1 is that it works fairly well even if the potential is discontinuous. In this paper, we are going to prove the convergence of Method 1 for the model equation (1.13) when the potential is piecewise smooth and has a finite number of discontinuities at half numerical grid points. First, we nondimensionalize (1.13). The dimensionless independent variables and functions are defined as

$$\tilde{x} = x\frac{1}{L}, \qquad \tilde{t} = t\frac{D}{L^2},$$

$$\tilde{\psi}(\tilde{x}) = \psi(x)\frac{1}{k_B T}, \qquad \tilde{\rho}(\tilde{x}) = \rho(x)L, \qquad \Delta\tilde{\psi} = \Delta\psi\frac{1}{k_B T}.$$

Since we are going to work with the dimensionless variables and functions, let us drop $\sim$ from the notations. The dimensionless version of (1.13) is

$$\frac{\partial \rho}{\partial t} = \frac{\partial}{\partial x}\left[\psi'(x)\rho + \frac{\partial \rho}{\partial x}\right], \tag{1.14}$$

where $\psi(x)$ satisfies

$$\psi(x+1) = \psi(x) - \Delta\psi, \qquad \Delta\psi > 0.$$

Equation (1.14) can be viewed as a special case of (1.13) with $L = 1$, $D = 1$, and $k_B T = 1$.

The rest of the paper is organized as follows. In section 2, we discuss the two conditions that the exact solution of a discontinuous Fokker–Planck equation must satisfy at a discontinuity. We derive the two conditions for the exact solution at a discontinuity by rewriting the Fokker–Planck equation as a heat equation with discontinuous heat conductivity and discontinuous specific heat capacity. The first condition is the continuity of the "heat flux," which corresponds to the conservation of heat. The second condition is the continuity of the "temperature," which follows from the regularizing properties of the heat equation. In section 3, we describe the construction and properties of Method 1 developed in [16]. The most important property of Method 1 is that it preserves detailed balance. In section 4, we prove that Method 1 is stable with respect to a norm that is equivalent to the 2-norm. We start by showing that the steady state solution of the half discrete method is unique and all positive. This allows us to define a weighted 2-norm using the steady state solution as the weight function. We proceed to show that the steady state solution is bounded away from 0 and from infinity, independent of the numerical grid size. It follows that the weighted 2-norm is equivalent to the standard 2-norm. We then show that with respect to the weighted 2-norm, Method 1 is unconditionally stable. In section 5, we analyze the consistency of Method 1 when the potential is discontinuous. We show that away from the discontinuity, the local truncation error of Method 1 on the exact solution is $O(k(k^2+h^2))$. At the discontinuity, the local truncation error on the exact solution is $O(1)$. However, if we perturb the exact solution by a term of the order $O(h)$, then the local truncation error on the perturbed solution is $O(k(k^2+h))$. Once we have both the stability and consistency, the Lax equivalence theorem [17] implies that Method 1 converges to the correct solution of the differential equation. In section 6, we propose a modified version of Method 1 to eliminate the first order error term caused by the discontinuity (hereafter referred to as Method 2). As a result, the modified method (Method 2) is second order accurate even in the presence of discontinuities. In section 7, we carry out numerical simulations using a discontinuous potential to compare the performance of the central difference method, Method 1, and Method 2. The central difference method converges to a wrong solution. Both Method 1 and Method 2 converge to the correct solution. We also show that in the presence of discontinuities, detailed balance is a necessary condition for converging to the correct solution. This explains the defect of the central difference method.

2. Exact solution of a discontinuous Fokker–Planck equation and conditions at the discontinuity. In this section, we discuss the two conditions that the exact solution of a discontinuous Fokker–Planck equation must satisfy at a discontinuity. We derive the two conditions for the exact solution at a discontinuity by rewriting the Fokker–Planck equation as a heat equation with discontinuous heat conductivity and discontinuous specific heat capacity. The first condition is the continuity of the "heat flux." The second condition is the continuity of the "temperature."

We study the case where potential $\psi(x)$ is piecewise smooth and has a finite number of discontinuities in one period. Without loss of generality, we assume that there is only one discontinuity at x_d in $[0, 1]$. More specifically, we assume that $\psi(x)$ is two smooth functions connected by the discontinuity. That is, $\psi(x)$ is smooth in

$[0, x_d]$ if $\psi(x_d)$ is redefined as $\psi(x_d) = \lim_{x \to x_d^-} \psi(x)$, and $\psi(x)$ is smooth in $[x_d, 1]$ if $\psi(x_d)$ is redefined as $\psi(x_d) = \lim_{x \to x_d^+} \psi(x)$. For simplicity, in this paper a smooth function means it is infinitely differentiable, and so we can use as many terms of its Taylor expansion as we want.

When $\psi(x)$ is discontinuous at x_d, $\psi'(x)$ is not a regular function. If the system is brought to an equilibrium, the equilibrium solution is given by the Boltzmann distribution:

$$\rho(x) = \frac{1}{Z} e^{-\psi(x)}, \qquad Z = \int_0^1 e^{-\psi(x)} dx,$$

which is discontinuous at x_d. Thus, we should expect $\rho(x,t)$ to be discontinuous as a function of x at x_d. In modeling molecular motors, a discontinuous potential is simply a mathematical abstraction. In reality, the discontinuity represents a very narrow transition region in which the potential is smooth but changes dramatically. When the potential is smooth, we can rewrite Fokker–Planck equation (1.14) as

$$\frac{\partial \rho}{\partial t} = \frac{\partial}{\partial x} \left(e^{-\psi(x)} \frac{\partial e^{\psi(x)} \rho}{\partial x} \right). \tag{2.1}$$

Let us introduce $u(x,t) \equiv e^{\psi(x)} \rho(x,t)$. The equation above can be written in the form

$$\frac{\partial e^{-\psi(x)} u}{\partial t} = \frac{\partial}{\partial x} \left(e^{-\psi(x)} \frac{\partial u}{\partial x} \right). \tag{2.2}$$

Equation (2.2) has the form of a heat equation. In (2.2), $u(x,t)$ can be viewed as the "temperature," $e^{-\psi(x)}$ on the right-hand side as the heat conductivity, $e^{-\psi(x)}$ on the left-hand side as the specific heat capacity, and $e^{-\psi(x)} u(x,t) = \rho(x,t)$ as the heat. Equation (2.2) is equivalent to Fokker–Planck equation (1.14) when the potential is smooth. So it is natural for us to use the exact solution of (2.2) to define the exact solution of Fokker–Planck equation (1.14) when the potential is discontinuous. The biggest advantage of using (2.2) is that we can avoid the nonconservative product $\psi'(x)\rho(x,t)$ in Fokker–Planck equation (1.14). When both $\psi(x)$ and $\rho(x,t)$ are discontinuous, it is highly nontrivial to interpret the nonconservative product $\psi'(x)\rho(x,t)$ in Fokker–Planck equation (1.14) (for example, in [23], nonconservative product of the form $\frac{dw}{dx} g(w)$ is defined as a Borel measure).

In (2.2), when $\psi(x)$ is discontinuous, both the heat conductivity and the specific heat capacity are discontinuous. Away from the discontinuity, the exact solution of (2.2) satisfies differential equation (2.2) in the classical sense. At the discontinuity, the exact solution of (2.2) is constrained by two conditions. The first condition is the continuity of the "heat flux," which corresponds to the conservation of heat. The second condition is the continuity of the "temperature," which follows from the regularizing properties of the heat equation. The continuity of the "temperature" also reflects the physical nature of the heat conduction process: temperature gradient is relaxed by the heat flow that is induced by the temperature gradient. In particular, any isolated discontinuity in temperature will be removed immediately by heat conduction.

Now we write the two conditions in terms of $\rho(x,t)$ and $\psi(x)$. The first condition (continuity of "heat flux") is

$$\left(\psi'(x)\rho + \frac{\partial \rho}{\partial x} \right) \Big|_{x = x_d^-} = \left(\psi'(x)\rho + \frac{\partial \rho}{\partial x} \right) \Big|_{x = x_d^+}. \tag{2.3}$$

For Fokker–Planck equation (1.14), condition (2.3) means that the probability flux into the discontinuity is the same as the probability flux out of the discontinuity (i.e., the conservation of probability at the discontinuity), which corresponds to the well-known Rankine–Hugoniot condition for weak solutions of hyperbolic equations [24]. The second condition (continuity of "temperature") is

$$\left(e^{\psi(x)}\rho(x,t)\right)\Big|_{x=x_d^-} = \left(e^{\psi(x)}\rho(x,t)\right)\Big|_{x=x_d^+}. \tag{2.4}$$

Equations (2.3) and (2.4) are the two conditions that the exact solution of a discontinuous Fokker–Planck equation must satisfy at the discontinuity. If a numerical method is based on conservation of probability, then the numerical solution will automatically satisfy condition (2.3). As we will see in section 7, condition (2.4) is related to detailed balance. If a numerical method does not preserve detailed balance, then the numerical solution may converge to a wrong solution that does not satisfy condition (2.4).

3. The numerical method. In this section, we summarize Method 1 proposed in [16]. In the spatial discretization of (1.14), we divide the period $[0,1]$ into M subintervals of size $h = 1/M$. Each subinterval is represented by its center (a site), and the numerical grid is formed as

$$h = \frac{1}{M}, \qquad x_j = \frac{h}{2} + jh, \qquad x_{j-1/2} = \frac{h}{2} + \left(j - \frac{1}{2}\right) h.$$

Since the underlying stochastic evolution (1.12) is a continuous Markov process, we discretize it as a jump process (discrete Markov process). The idea of using a jump process on discrete sites to approximate a continuous Markov process was originated in [18] and in an unpublished result by C. Peskin. As shown in Figure 3.1, in the spatial discretization, subinterval j is $\left[x_{j-1/2}, x_{j+1/2}\right]$ and its center is x_j. The motor system can reside only on a set of discrete sites $\{x_j\}$. In a single jump, it can jump only to one of the two adjacent sites. Let $h \cdot p_j(t)$ be the probability that the motor system is at site x_j at time t in the jump process. $p_j(t)$ can be viewed as

$$p_j(t) \approx \frac{1}{h}\int_{x_{j-1/2}}^{x_{j+1/2}} \rho(x,t)dx \approx \rho(x_j,t). \tag{3.1}$$

Let $F_{j+1/2}$ be the rate of jumping from x_j to x_{j+1} (forward jump) and $B_{j+1/2}$ the rate of jumping from x_{j+1} to x_j (backward jump). The numerical probability flux through $x_{j+1/2}$ is

$$J_{j+1/2} = h\left(F_{j+1/2}\, p_j - B_{j+1/2}\, p_{j+1}\right). \tag{3.2}$$

The time evolution of $p_j(t)$ is governed by the conservation of probability:

$$\begin{aligned} \frac{dp_j}{dt} &= \frac{1}{h}\left(J_{j-1/2} - J_{j+1/2}\right) \\ &= \left(F_{j-1/2}\, p_{j-1} - B_{j-1/2}\, p_j\right) - \left(F_{j+1/2}\, p_j - B_{j+1/2}\, p_{j+1}\right). \end{aligned} \tag{3.3}$$

Before we describe how the jump rates $F_{j+1/2}$ and $B_{j+1/2}$ are calculated in Method 1, we would like to point out that (3.3) is a very general framework. It can even accommodate the central difference method, which can be cast into the form of (3.3) with

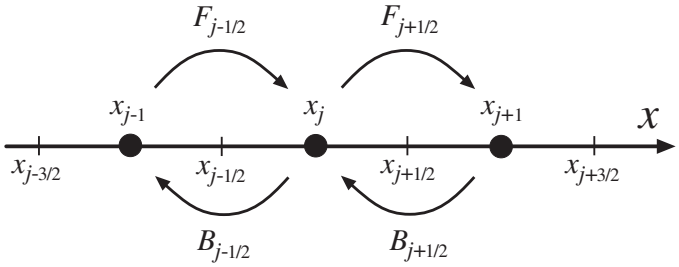

FIG. 3.1. *Spatial discretization of* (1.14). *The motor system is restricted to a set of discrete sites* $\{x_j\}$ *and can jump only to adjacent sites.*

jump rates

$$F_{j+1/2}^{(CD)} = \frac{1}{h^2}\left(1 - \frac{\delta\psi_{j+1/2}}{2}\right),$$
$$B_{j+1/2}^{(CD)} = \frac{1}{h^2}\left(1 + \frac{\delta\psi_{j+1/2}}{2}\right), \tag{3.4}$$

where

$$\delta\psi_{j+1/2} = \psi(x_{j+1}) - \psi(x_j). \tag{3.5}$$

Notice, however, that the jump rates (3.4) associated with the central difference method may be negative. Even in the limit of $h \to 0$, the jump rates (3.4) may be negative when the potential $\psi(x)$ is discontinuous. This explains why the central difference method converges to a wrong solution (as we will see in section 7).

In Method 1 [16], the jump rates are calculated based on local approximate solutions. In calculating $F_{j+1/2}$ and $B_{j+1/2}$, we make two assumptions:

1. In $[x_{j-1/2}, x_{j+3/2}]$, potential $\psi(x)$ is linear with slope $\delta\psi_{j+1/2}/h$. This assumption is to make the method simple and easy to implement. Under this assumption, the potential in $[x_{j-1/2}, x_{j+3/2}]$ is given by

$$\psi(x) = C + \frac{\delta\psi_{j+1/2}}{h} \cdot x, \tag{3.6}$$

   where $\delta\psi_{j+1/2}$ is defined in (3.5).

2. Let $\rho_{j+1/2}(x)$ be the steady state solution of (1.14) in $[x_{j-1/2}, x_{j+3/2}]$ with linear potential (3.6) and subject to the condition

$$\frac{1}{h}\int_{x_{j-1/2}}^{x_{j+1/2}} \rho_{j+1/2}(x)dx = p_j,$$
$$\frac{1}{h}\int_{x_{j+1/2}}^{x_{j+3/2}} \rho_{j+1/2}(x)dx = p_{j+1}. \tag{3.7}$$

   In the jump process, the probability flux through $x_{j+1/2}$ is given by that of $\rho_{j+1/2}(x)$. This assumption is a key component of Method 1 [16]. Instead of using the Taylor expansion, the numerical approximation is based on local approximate solutions. The consequence of this approach is that detailed balance is preserved, and Method 1 works well even if the potential is discontinuous.

The probability flux of $\rho_{j+1/2}(x)$ is derived in [16] and is given by

$$J = \frac{1}{h} \cdot \frac{\delta\psi_{j+1/2}}{e^{\delta\psi_{j+1/2}} - 1} \left(p_j - e^{\delta\psi_{j+1/2}}\, p_{j+1} \right). \tag{3.8}$$

Comparing the theoretical flux (3.8) with the numerical flux (3.2), we immediately obtain

$$\begin{aligned} F_{j+1/2} &= \frac{1}{h^2} \frac{\delta\psi_{j+1/2}}{e^{\delta\psi_{j+1/2}} - 1}, \\ B_{j+1/2} &= \frac{1}{h^2} \frac{\delta\psi_{j+1/2}\, e^{\delta\psi_{j+1/2}}}{e^{\delta\psi_{j+1/2}} - 1}, \end{aligned} \tag{3.9}$$

where $\delta\psi_{j+1/2} = \psi(x_{j+1}) - \psi(x_j)$, as defined in (3.5). It is important to notice that the jump rates (3.9) are always positive. It is straightforward to verify that $F_{j+1/2}$ and $B_{j+1/2}$ are both positive when $\delta\psi_{j+1/2} \neq 0$. When $\psi_{j+1/2} = 0$, we have

$$\begin{aligned} F_{j+1/2} &= \lim_{\delta\psi \to 0} \frac{1}{h^2} \frac{\delta\psi}{e^{\delta\psi} - 1} = \frac{1}{h^2}, \\ B_{j+1/2} &= \lim_{\delta\psi \to 0} \frac{1}{h^2} \frac{\delta\psi\, e^{\delta\psi}}{e^{\delta\psi} - 1} = \frac{1}{h^2}. \end{aligned}$$

The property that the jump rates given in (3.9) are always positive will be used in the stability analysis below. The jump rates given in (3.9) also satisfy detailed balance [16]:

$$\frac{F_{j+1/2}}{B_{j+1/2}} = e^{\psi(x_j) - \psi(x_{j+1})}. \tag{3.10}$$

In the time dimension, (3.3) is discretized using a Crank–Nicolson-type method [19]. Let p_j^n be the numerical approximation for $p_j(nk)$, where k is the time step. The fully discrete method is

$$\begin{aligned} p_j^{n+1} = p_j^n + k \Bigg\{ & \left(F_{j-1/2} \frac{p_{j-1}^n + p_{j-1}^{n+1}}{2} - B_{j-1/2} \frac{p_j^n + p_j^{n+1}}{2} \right) \\ & - \left(F_{j+1/2} \frac{p_j^n + p_j^{n+1}}{2} - B_{j+1/2} \frac{p_{j+1}^n + p_{j+1}^{n+1}}{2} \right) \Bigg\}. \end{aligned} \tag{3.11}$$

In the calculation of average velocity and/or effective diffusion coefficient, (1.14) is solved with the periodic boundary condition [16]. In the analysis of subsequent sections, we always assume the periodic boundary condition:

$$p_j^n = p_{j+M}^n, \qquad \psi(x+1) = \psi(x) - \Delta\psi.$$

We will prove the stability and consistency of (3.11) when potential $\psi(x)$ is piecewise smooth and has a finite number of discontinuities at half numerical grid points.

4. Stability of the numerical method. In this section, we prove the stability of Method 1 [16]. We first show that the steady state solution of the half discrete method (3.3) is unique and is all positive. Furthermore, we show that the maximum of the steady state solution is bounded by the minimum multiplied by a constant that

is determined by the underlying physical problem but is independent of the numerical grid size. Thus, we can define a weighted 2-norm using the steady state solution as the weighting function, and the weighted 2-norm so defined is equivalent to the 2-norm. Then we prove that the fully discrete method (3.11) is unconditionally stable with respect to the weighted 2-norm.

For the convenience of mathematical discussion, we introduce vector notations for numerical solutions in one period:

$$\begin{aligned}\vec{p}^{\,n} &\equiv (p_1^n,\ p_2^n,\ \ldots,\ p_M^n)\,,\\ \vec{q} &\equiv (q_1,\ q_2,\ \ldots,\ q_M)\,,\\ \vec{r} &\equiv (r_1,\ r_2,\ \ldots,\ r_M)\,.\end{aligned}$$

Here the superscript n denotes the time level. Remember all solutions are periodic. Let $\vec{q}$ be the steady state solution of (3.3). $\vec{q}$ satisfies the equation

$$(F_{j-1/2}\,q_{j-1} - B_{j-1/2}\,q_j) - (F_{j+1/2}\,q_j - B_{j+1/2}\,q_{j+1}) = 0, \qquad j = 1, 2, \ldots, M, \tag{4.1}$$

and satisfies the constraint

$$h\sum_{j=1}^{M} q_j = 1. \tag{4.2}$$

Condition (4.2) corresponds to $\int_0^1 \rho(x)dx = 1$. We now show that $\vec{q}$ is unique, is all positive, and is bounded away from 0 and from infinity, independent of the numerical grid size.

THEOREM 4.1. *Suppose $\vec{q}$ satisfies* (4.1). *Then $\vec{q}$ is either all zeros or all positive or all negative.*

Proof. Suppose $\vec{q}$ is not all zeros. Otherwise, there is no need to continue. Without loss of generality, we assume that there is an index j_0 such that $q_{j_0} > 0$. Otherwise, we simply consider $-\vec{q}$, which also satisfies (4.1). Starting at j_0, we first search to the left for a nonpositive element. If we cannot find a nonpositive element over a distance of M grid points, then all elements are positive because the solution is periodic.

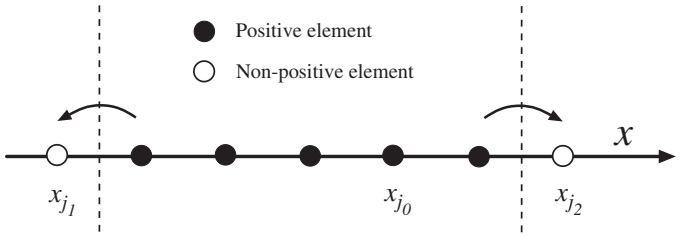

FIG. 4.1. *Starting from a positive element, $q_{j_0} > 0$, we either find that all elements are positive or find a positive region bounded by nonpositive elements. The latter leads to a contradiction.*

Suppose q_{j_1} is the first nonpositive element found in the search to the left and q_{j_2} is the first nonpositive element found in the search to the right. As shown in Figure 4.1, we have a positive region bounded by nonpositive elements:

$$q_{j_1} \le 0, \qquad q_{j_2} \le 0, \qquad \text{and } q_j > 0 \qquad \text{for } j_1 < j < j_2.$$

We are going to show that this leads to a contradiction. Summing (4.1) from $j = j_1+1$ to $j = j_2 - 1$, we obtain

$$\left(B_{j_1+1/2}\, q_{j_1+1} - F_{j_1+1/2}\, q_{j_1}\right) + \left(F_{j_2-1/2}\, q_{j_2-1} - B_{j_2-1/2}\, q_{j_2}\right) = 0. \tag{4.3}$$

The two terms on the left-hand side of (4.3) are the net probability fluxes to the outside of the region. Recall that the jump rates in Method 1 are always positive. Because $q_{j_1+1} > 0$ and $q_{j_1} \le 0$, the first term is positive. Similarly, the second term is also positive. Thus, the total net probability flux to the outside of the region is positive. This contradicts that $\vec{q}$ is a steady state. Mathematically, the contradiction arises in (4.3), where the two positive terms sum to zero. Therefore, if one element is positive, then all elements must be positive. ∎

Remark. The proof presented here can be extended to Fokker–Planck equations of higher dimensions, in which the positive region is bounded by a combination of nonpositive elements and a periodic boundary. The total net probability flux to the outside of the region is positive, which contradicts the steady state assumption.

THEOREM 4.2. *Suppose $\vec{q}$ satisfies* (4.1) *and* (4.2). *Then $\vec{q}$ is unique and all positive.*

Proof. Suppose both $\vec{q}$ and $\vec{p}$ satisfy (4.1) and (4.2). Let $\vec{r} = \vec{q} - \vec{p}$. Then $\vec{r}$ satisfies (4.1). Applying Theorem 4.1 to $\vec{r}$ yields that $\vec{r}$ is either all zeros or all positive or all negative. Since $\vec{r}$ also satisfies $h\sum_{j=1}^{M} r_j = 0$, $\vec{r}$ must be all zeros. Consequently, $\vec{q}$ is unique. Applying Theorem 4.1 to $\vec{q}$ and using (4.2), we obtain that $\vec{q}$ is all positive. ∎

Remark. This theorem shows that the solution of (4.1) with condition (4.2) is unique and all positive. In other words, Method 1 yields a unique steady state solution and preserves the positivity of probability. As pointed above, this result can be extended to Fokker–Planck equations of higher dimensions.

Now we consider the 2-norm and the weighted 2-norm defined as

$$\|\vec{p}\|_2 \equiv \left(h\sum_{j=1}^{M} (p_j)^2\right)^{\frac{1}{2}},$$

$$\|\vec{p}\|_\psi \equiv \left(h\sum_{j=1}^{M} \frac{1}{q_j}\,(p_j)^2\right)^{\frac{1}{2}}, \qquad h = \frac{1}{M}, \tag{4.4}$$

where $\vec{q} = (q_1,\ q_2,\ \ldots,\ q_M)$ is the solution of (4.1) with condition (4.2). In the analysis below, $\vec{q} = (q_1,\ q_2,\ \ldots,\ q_M)$ is reserved to denote this steady state solution. The 2-norm is denoted by $\|\bullet\|_2$. The weighted 2-norm is denoted by $\|\bullet\|_\psi$ because the weighting function $\vec{q}$ depends on potential $\psi(x)$.

THEOREM 4.3. *Suppose the free energy drop satisfies $\Delta\psi = \psi(x) - \psi(x+1) > 0$. Then the steady state probability flux of* (4.1), *$\tilde{J} = h\left(F_{j+1/2}\, q_j - B_{j+1/2}\, q_{j+1}\right)$, must be positive.*

Proof. We use proof by contradiction. Suppose $\tilde{J} \le 0$. Recall that Method 1 satisfies detailed balance (3.10). It follows that

$$q_{j+1} \ \ge\ \frac{F_{j+1/2}}{B_{j+1/2}}\, q_j = e^{\psi(x_j)-\psi(x_{j+1})}\, q_j.$$

Applying the inequality for $j,\ j+1,\ \ldots$, we obtain

$$q_{j+M} \ \ge\ e^{\psi(x_j)-\psi(x_{j+M})}\, q_j = e^{\Delta\psi}\, q_j > q_j,$$

which contradicts the periodic condition $q_{j+M} = q_j$. In the above, we have used the condition $\Delta\psi > 0$. Therefore, when $\Delta\psi$ is positive, $\tilde{J}$ must be positive. ∎

Remark. The key component in the proof of this theorem is detailed balance (3.10). A method preserving detailed balance has the advantage that the direction of chemical reaction and mechanical motion is preserved in numerical results. That is, the method will not produce a numerical result in which the motor system goes upward along the free energy landscape. This property is very important in studies of molecular motors.

THEOREM 4.4. *Suppose $\Delta\psi > 0$, and $\vec{q}$ satisfies* (4.1) *and* (4.2). *Then we have*

$$\max_j q_j \le e^{C_\psi}, \qquad \min_j q_j \ge e^{-C_\psi}, \tag{4.5}$$

where C_ψ depends on potential $\psi(x)$ but is independent of the numerical grid size.

Proof. Equation (4.1) implies that

$$\left(F_{j+1/2}\, q_j - B_{j+1/2}\, q_{j+1}\right) = \frac{\tilde{J}}{h}, \quad \text{independent of } j, \tag{4.6}$$

where $\tilde{J}$ is the steady state probability flux. Applying Theorem 4.3, we have $\tilde{J} > 0$, and (4.6) becomes

$$\left(F_{j+1/2}\, q_j - B_{j+1/2}\, q_{j+1}\right) \ge 0.$$

Recall that Method 1 satisfies detailed balance (3.10). It follows that

$$q_{j+1} \;\le\; \frac{F_{j+1/2}}{B_{j+1/2}}\, q_j = e^{\psi(x_j)-\psi(x_{j+1})}\, q_j. \tag{4.7}$$

Let $q_l = \min_j q_j$. Applying inequality (4.7) for $j = l$, $j = l+1$, ..., we get

$$q_j \;\le\; e^{\psi(x_l)-\psi(x_j)}\, q_l \quad \text{for } j \ge l. \tag{4.8}$$

Let $C_\psi = \max_x \max_{x\le y\le x+1} (\psi(x) - \psi(y))$. C_ψ is a constant independent of the numerical grid size. Taking the maximum of both sides of (4.8) over $l \le j \le l + M$, and noticing that $\vec{q}$ is periodic, we obtain

$$\max_j q_j \;\le\; e^{C_\psi}\, q_l = e^{C_\psi} \min_j q_j. \tag{4.9}$$

Since $\vec{q}$ also satisfies (4.2), we have

$$\min_j q_j \le h \sum_{j=1}^{M} q_j = 1, \qquad \max_j q_j \ge h \sum_{j=1}^{M} q_j = 1. \tag{4.10}$$

Equations (4.9) and (4.10) lead immediately to (4.5). ∎

Remark. This theorem shows that the weighted 2-norm is equivalent to the 2-norm

$$e^{-C_\psi} \|\vec{p}\|_2 \;\le\; \|\vec{p}\|_\psi \;\le\; e^{C_\psi} \|\vec{p}\|_2. \tag{4.11}$$

The extension of this theorem to Fokker–Planck equations of higher dimensions is still an open problem (we believe the theorem is valid for Fokker–Planck equations of higher dimensions, but the proof is still an open problem). We are going to use the weighted 2-norm to study the stability of the fully discrete method (3.11).

THEOREM 4.5. *Let $\vec{p}^{\,n} = (p_1^n, p_2^n, \ldots, p_M^n)$ denote the solution of the fully discrete method* (3.11) *at time level n. Then we have*

$$\|\vec{p}^{\,n+1}\|_\psi \le \|\vec{p}^{\,n}\|_\psi. \tag{4.12}$$

Proof. First, we write (3.11) as

$$p_j^{n+1} - p_j^n = \frac{k}{h}\left(J_{j-1/2}^{n+1/2} - J_{j+1/2}^{n+1/2}\right), \tag{4.13}$$

where

$$J_{j+1/2}^{n+1/2} = h\left(F_{j+1/2}\, p_j^{n+1/2} - B_{j+1/2}\, p_{j+1}^{n+1/2}\right), \tag{4.14}$$

$$p_j^{n+1/2} = \frac{p_j^{n+1} + p_j^n}{2}.$$

Multiplying both sides of (4.13) by $2\,h\,p_j^{n+1/2}$, dividing by q_j, and summing over j yields

$$h\sum_{j=1}^{M}\frac{1}{q_j}\,(p_j^{n+1})^2 - h\sum_{j=1}^{M}\frac{1}{q_j}\,(p_j^n)^2 = 2k\sum_{j=1}^{M}\frac{1}{q_j}p_j^{n+1/2}\left(J_{j-1/2}^{n+1/2} - J_{j+1/2}^{n+1/2}\right).$$

Applying summation by parts and using the periodic condition, we get

$$\|\vec{p}^{\,n+1}\|_\psi^2 - \|\vec{p}^{\,n}\|_\psi^2 = -2k\sum_{j=1}^{M}\left(\frac{1}{q_j}p_j^{n+1/2} - \frac{1}{q_{j+1}}p_{j+1}^{n+1/2}\right)J_{j+1/2}^{n+1/2}. \tag{4.15}$$

Let $r_j = \frac{p_j^{n+1/2}}{q_j}$. Here, for simplicity and without causing confusion, we have dropped the superscript $(n+1/2)$ from r_j. We write the probability flux $J_{j+1/2}^{n+1/2}$ as

$$\begin{aligned} J_{j+1/2}^{n+1/2} &= h\left(F_{j+1/2}\, p_j^{n+1/2} - B_{j+1/2}\, p_{j+1}^{n+1/2}\right) \\ &= h\left(F_{j+1/2}\, q_j\, r_j - B_{j+1/2}\, q_{j+1}\, r_{j+1}\right) \\ &= h\left(\frac{F_{j+1/2}\, q_j + B_{j+1/2}\, q_{j+1}}{2}\right)(r_j - r_{j+1}) + \tilde{J}\cdot\frac{r_j + r_{j+1}}{2}. \end{aligned}$$

Here $\tilde{J} = h\left(F_{j+1/2}\, q_j - B_{j+1/2}\, q_{j+1}\right)$ is the steady state probability flux, which is a constant independent of j. Substituting $J_{j+1/2}^{n+1/2}$ into (4.15), we have

$$\begin{aligned} \|\vec{p}^{\,n+1}\|_\psi^2 - \|\vec{p}^{\,n}\|_\psi^2 = &-kh\sum_{j=1}^{M}\left(F_{j+1/2}\, q_j + B_{j+1/2}\, q_{j+1}\right)(r_j - r_{j+1})^2 \\ &- k\sum_{j=1}^{M}\tilde{J}\left((r_j)^2 - (r_{j+1})^2\right). \end{aligned} \tag{4.16}$$

Recall that in Method 1, the steady state solution $\vec{q}$ is all positive and jump rates are all positive. Consequently, the first term on the right-hand side of (4.16) is nonpositive.

Applying summation by parts and using the periodic condition, we obtain that the second term on the right-hand side of (4.16) is zero. Thus, we conclude that

$$\|\vec{p}^{\,n+1}\|_\psi^2 - \|\vec{p}^{\,n}\|_\psi^2 \le 0, \tag{4.17}$$

which immediately leads to (4.12). □

Remark 1. This theorem shows that the fully discrete method (3.11) is unconditionally stable with respect to the weighted 2-norm $\| \bullet \|_\psi$ even if potential $\psi(x)$ is discontinuous.

Remark 2. This theorem can be extended to Fokker–Planck equations of higher dimensions.

5. Consistency and convergence of the numerical method. We study the consistency of Method 1 when potential $\psi(x)$ is piecewise smooth and has a finite number of discontinuities in one period at half numerical grid points. Without loss of generality, we assume that there is only one discontinuity at x_d in $[0,1]$, where $x_d = x_{l+1/2}$ is a half numerical grid point (that is, x_d is at the boundary between two numerical subintervals). Below we will show that away from the discontinuity, the local truncation error of Method 1 on the exact solution is $O\left(k(k^2+h^2)\right)$. At the discontinuity, the local truncation error on the exact solution is $O(1)$. However, if we perturb the exact solution by a term of the order $O(h)$, then the local truncation error on the perturbed solution (instead of the exact solution) is $O\left(k(k^2+h)\right)$.

5.1. Local truncation error away from the discontinuity. We rewrite the fully discrete method (3.11) in the flux form

$$p_j^{n+1} = p_j^n + \frac{k}{h}\left(\frac{J_{j-1/2}^n + J_{j-1/2}^{n+1}}{2} - \frac{J_{j+1/2}^n + J_{j+1/2}^{n+1}}{2}\right), \tag{5.1}$$

where the numerical probability flux is

$$J_{j+1/2}^n = h\left(F_{j+1/2}\, p_j^n - B_{j+1/2}\, p_{j+1}^n\right). \tag{5.2}$$

Let $\rho(x,t)$ be the exact solution of (1.14) subject to conditions (2.3) and (2.4). Let ρ_j^n denote the exact solution on the numerical grid:

$$\rho_j^n = \rho(x_j, t_n).$$

The local truncation error is defined as the residual term when the numerical method is applied to the exact solution ρ_j^n. Integrating the differential equation (1.14) over $[x_{j-1/2}, x_{j+1/2}] \times [t_n, t_{n+1}]$, we have

$$\begin{aligned}\int_{x_{j-1/2}}^{x_{j+1/2}} \rho(x,t_{n+1})dx - \int_{x_{j-1/2}}^{x_{j+1/2}} \rho(x,t_n)dx \\ = \int_{t_n}^{t_{n+1}} J(x_{j-1/2},t)dt - \int_{t_n}^{t_{n+1}} J(x_{j+1/2},t)dt,\end{aligned} \tag{5.3}$$

where $J(x,t) = -\left(\psi'\rho + \frac{\partial \rho}{\partial x}\right)$ is the exact probability flux in (1.14). Using the trapezoidal rule to approximate the integrals on the right-hand side yields

$$\begin{aligned}\int_{t_n}^{t_{n+1}} J(x_{j+1/2},t)dt = k\left(\frac{J(x_{j+1/2},t_n) + J(x_{j+1/2},t_{n+1})}{2}\right) \\ - \frac{k^3}{12}\frac{\partial^2}{\partial t^2} J(x_{j+1/2}, t_{n+1/2}) + O(k^5).\end{aligned}$$

Since the probability flux, $J(x,t)$, is continuous across the discontinuity, the time derivatives of $J(x,t)$ are also continuous across the discontinuity. Suppose $x_{j+1/2}$ is the location of discontinuity. Then we have

$$\frac{\partial^2}{\partial t^2} J(x^+_{j+1/2}, t_{n+1/2}) = \frac{\partial^2}{\partial t^2} J(x^-_{j+1/2}, t_{n+1/2}).$$

Using the assumption that everything is smooth on both sides of the discontinuity, we obtain

$$\begin{aligned}\frac{\partial^2}{\partial t^2} J(x^-_{j+1/2}, t_{n+1/2}) - \frac{\partial^2}{\partial t^2} J(x_{j-1/2}, t_{n+1/2}) \\ = h \frac{\partial^3}{\partial t^2 \partial x} J(\xi, t_{n+1/2}) = O(h),\end{aligned}$$

where $x_{j-1/2} < \xi < x_{j+1/2}$. Expanding the integrals on the left-hand side of (5.3), using the results we just derived for the integrals on the right-hand side of (5.3), and then dividing (5.3) by h, we arrive at

$$\begin{aligned}\rho_j^{n+1} - \rho_j^n = \frac{k}{h} \Bigg(& \frac{J(x_{j-1/2}, t_n) + J(x_{j-1/2}, t_{n+1})}{2} \\ & - \frac{J(x_{j+1/2}, t_n) + J(x_{j+1/2}, t_{n+1})}{2} \Bigg) + O\left(k(k^2 + h^2)\right).\end{aligned} \tag{5.4}$$

Let $J^n_{j+1/2}\{\rho\}$ denote the numerical probability flux on the exact solution $\rho(x,t)$:

$$J^n_{j+1/2}\{\rho\} = h\left(F_{j+1/2}\, \rho_j^n - B_{j+1/2}\, \rho_{j+1}^n\right). \tag{5.5}$$

We expand $F_{j+1/2}$, $B_{j+1/2}$, ρ_j^n, and ρ_j^{n+1} around $x = x_{j+1/2}$ to obtain the following expansion for $J^n_{j+1/2}\{\rho\}$ away from the discontinuity:

$$J^n_{j+1/2}\{\rho\} = J(x_{j+1/2}, t_n) - h^2\, u(x_{j+1/2}, t_n) + O\left(h^3\right), \tag{5.6}$$

where $u(x,t)$ is a function consisting of various derivatives of $\psi(x)$ and $\rho(x,t)$. The derivation of (5.6) is presented in Appendix A. Notice that $u(x,t)$ is smooth in the region where $\psi(x)$ and $\rho(x,t)$ are smooth. Away from the discontinuity, $u(x,t)$ satisfies

$$u(x_{j+1/2}, t_n) - u(x_{j-1/2}, t_n) = O(h).$$

Substituting (5.6) into (5.4), we obtain that, away from the discontinuity, ρ_j^n satisfies

$$\begin{aligned}\rho_j^{n+1} = \rho_j^n + \frac{k}{h} \left(\frac{J^n_{j-1/2}\{\rho\} + J^{n+1}_{j-1/2}\{\rho\}}{2} - \frac{J^n_{j+1/2}\{\rho\} + J^{n+1}_{j+1/2}\{\rho\}}{2} \right) \\ + O\left(k(k^2 + h^2)\right).\end{aligned} \tag{5.7}$$

That is, away from the discontinuity, the local truncation error on the exact solution $\rho(x,t)$ is $O\left(k(k^2 + h^2)\right)$.

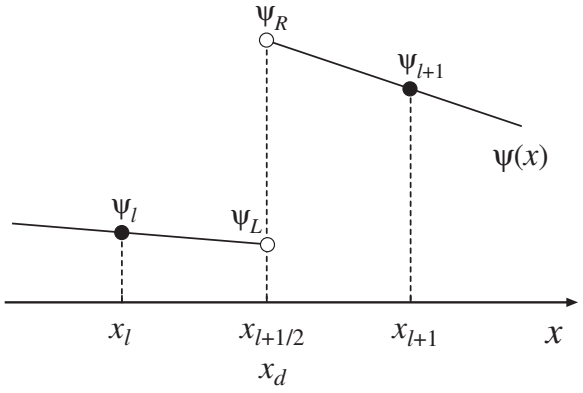

FIG. 5.1. *Schematic diagram of the discontinuity at* $x_d = x_{l+1/2}$.

5.2. Local truncation error on the perturbed solution. Now let us look at the numerical probability flux at the discontinuity. As shown in Figure 5.1, the discontinuity is at $x_d = x_{l+1/2}$. We introduce several shorthand notations:

$$\rho_L^n = \rho(x,t_n)|_{x=x_d^-}\,, \qquad \rho_R^n = \rho(x,t_n)|_{x=x_d^+}\,,$$

$$\psi_L = \psi(x)|_{x=x_d^-}\,, \qquad \psi_R = \psi(x)|_{x=x_d^+}\,.$$

The numerical probability flux on the exact solution $\rho(x,t)$ is

$$\begin{aligned} J_{l+1/2}^n\{\rho\} &= h\left(F_{l+1/2}\rho_l^n - B_{l+1/2}\rho_{l+1}^n\right) \\ &= \frac{1}{h}\,\frac{\psi_{l+1}-\psi_l}{e^{\psi_{l+1}}-e^{\psi_l}}\left(e^{\psi_l}\rho_l^n - e^{\psi_{l+1}}\rho_{l+1}^n\right) \\ &= \frac{1}{h}\,\frac{\psi_{l+1}-\psi_l}{e^{\psi_{l+1}}-e^{\psi_l}}\left(e^{\psi_l}\rho_l^n - e^{\psi_L}\rho_L^n + e^{\psi_R}\rho_R^n - e^{\psi_{l+1}}\rho_{l+1}^n\right). \end{aligned} \tag{5.8}$$

Here we have used condition (2.4): $e^{\psi_L}\rho_L^n = e^{\psi_R}\rho_R^n$. Expanding $e^{\psi_l}\rho_l^n$ around $x = x_d^-$ and $e^{\psi_{l+1}}\rho_{l+1}^n$ around $x = x_d^+$, we get

$$\begin{aligned} &e^{\psi_l}\rho_l^n - e^{\psi_L}\rho_L^n \\ &\quad= -\frac{h}{2}e^{\psi_L}\left(\psi'(x)\rho + \frac{\partial\rho}{\partial x}\right)\bigg|_{x=x_d^-} + h^2\,v_L(t_n) + h^3\,w_L(t_n) + O(h^4) \\ &\quad= \frac{h}{2}e^{\psi_L}J(x_{l+1/2},t_n) + h^2\,v_L(t_n) + h^3\,w_L(t_n) + O(h^4), \end{aligned}$$

$$\begin{aligned} &e^{\psi_R}\rho_R^n - e^{\psi_{l+1}}\rho_{l+1}^n \\ &\quad= \frac{h}{2}e^{\psi_R}J(x_{l+1/2},t_n) + h^2\,v_R(t_n) + h^3\,w_R(t_n) + O(h^4), \end{aligned}$$

where $v_L(t)$, $v_R(t)$, $w_L(t)$, and $w_R(t)$ are smooth functions of t. Substituting these two expansions into (5.8), we have

$$J_{l+1/2}^n\{\rho\} = J(x_{l+1/2},t_n) + v_0(t_n) + h\,v_1(t_n) + h^2\,v_2(t_n) + O(h^3), \tag{5.9}$$

where

$$v_0(t) = \left[\frac{\psi_R - \psi_L}{e^{\psi_R} - e^{\psi_L}}\left(\frac{e^{\psi_L} + e^{\psi_R}}{2}\right) - 1\right] J(x_{l+1/2}, t_n). \tag{5.10}$$

Again, $v_0(t)$, $v_1(t)$, and $v_2(t)$ are smooth functions of t. Combining (5.9), which gives numerical flux at the discontinuity, and (5.6), which is valid away from the discontinuity, we obtain

$$\begin{aligned} J^n_{j-1/2}\{\rho\} - J^n_{j+1/2}\{\rho\} &= \big(J(x_{j-1/2}, t_n) - J(x_{j+1/2}, t_n)\big) + O(h^3) \\ &+ h^2\left(u(x_d^+, t_n) - u(x_d^-, t_n)\right) a_j + h\left(v_0(t_n) + h\, v_1(t_n) + h^2 \tilde{v}_2(t_n)\right) b_j, \end{aligned} \tag{5.11}$$

where

$$a_j = \begin{cases} \frac{1}{2}, & j = l, \\ \frac{1}{2}, & j = l+1, \\ -h\frac{M}{M-2} & \text{otherwise}, \end{cases} \tag{5.12}$$

$$b_j = \begin{cases} -\frac{1}{h}, & j = l, \\ +\frac{1}{h}, & j = l+1, \\ 0 & \text{otherwise}, \end{cases} \tag{5.13}$$

and

$$\tilde{v}_2(t) = v_2(t) + \frac{u(x_d^+, t) + u(x_d^-, t)}{2}. \tag{5.14}$$

In (5.11), the first term on the right-hand side is the desired result; the second term is of the order $O(h^3)$; the third term is of the order $O(h^2)$ at the discontinuity and of the order $O(h^3)$ elsewhere; the fourth term is of the order $O(1)$, which is the term we need to deal with.

Terms in (5.11) contribute to the local truncation error. In general, the global error is one order lower than the local truncation error. However, the $O(1)$ term in (5.11) does not necessarily imply that the error in the numerical solution is $O(1/h)$ or is $O(1)$. As we will see below, the $O(1)$ term in (5.11) actually leads to an $O(h)$ term in the global error. The key is that the $O(1)$ term in (5.11) can be eliminated by perturbing the exact solution by an $O(h)$ term. So if we use the perturbed exact solution to calculate the local truncation error, then the $O(1)$ term in (5.11) disappears. In other words, the numerical method is consistent with the perturbed exact solution and the perturbed exact solution converges to the exact solution. The successful elimination of the $O(1)$ term in (5.11) by perturbing the exact solution by an $O(h)$ term depends on the special structure of vector $\{b_j\}$ given in (5.13). For that purpose, we have the theorem below.

THEOREM 5.1. *Suppose $\vec{r}$ is periodic, satisfies the equation*

$$h\left(F_{j-1/2}\, r_{j-1} - B_{j-1/2}\, r_j\right) - h\left(F_{j+1/2}\, r_j - B_{j+1/2}\, r_{j+1}\right) = b_j, \tag{5.15}$$

and satisfies the condition

$$\sum_{j=1}^{M} r_j = 0, \tag{5.16}$$

where b_j is defined in (5.13). *Then there exists a constant C_b, independent of the numerical grid size, such that*

$$\max_j |r_j| \le C_b.$$

Proof. The proof of Theorem 5.1 is presented in Appendix B. ∎

Now we use the result of Theorem 5.1 to eliminate the $O(1)$ error term in (5.11), and we consider the perturbed solution given below:

$$\tilde{\rho}_j^n \equiv \rho_j^n - h\left(v_0(t_n) + h\, v_1(t_n) + h^2\, \tilde{v}_2(t_n)\right) r_j = \rho_j^n + O(h), \tag{5.17}$$

where r_j is the solution of (5.15) and (5.16) in Theorem 5.1. It is straightforward to verify that the perturbed solution $\tilde{\rho}_j^n$ satisfies

$$J_{j-1/2}^n\{\tilde{\rho}\} - J_{j+1/2}^n\{\tilde{\rho}\} = \left(J(x_{j-1/2}, t_n) - J(x_{j+1/2}, t_n)\right) + O(h^2), \tag{5.18}$$

$$\tilde{\rho}_j^{n+1} - \tilde{\rho}_j^n = \rho_j^{n+1} - \rho_j^n + O(kh). \tag{5.19}$$

Substituting (5.18) and (5.19) into (5.4), we obtain

$$\begin{aligned}\tilde{\rho}_j^{n+1} = \tilde{\rho}_j^n + \frac{k}{h}\left(\frac{J_{j-1/2}^n\{\tilde{\rho}\} + J_{j-1/2}^{n+1}\{\tilde{\rho}\}}{2} - \frac{J_{j+1/2}^n\{\tilde{\rho}\} + J_{j+1/2}^{n+1}\{\tilde{\rho}\}}{2}\right)\\ + O\left(k(k^2+h)\right).\end{aligned} \tag{5.20}$$

That is, the local truncation error on the perturbed solution $\tilde{\rho}_j^n$ is $O\left(k(k^2+h)\right)$.

5.3. Convergence of the numerical method. Once we have both the stability and the consistency, the convergence follows, in principle, from the Lax equivalence theorem [17]. More specifically, we write the numerical method (3.11) in the vector-operator form

$$\vec{p}^{\,n+1} = L\,\vec{p}^{\,n}, \tag{5.21}$$

where L is the linear operator representing the numerical method. Stability (4.12) implies

$$\|L\|_\psi \le 1, \tag{5.22}$$

where $\|L\|_\psi$ is the induced operator norm defined by

$$\|L\|_\psi \equiv \max_{\|\vec{p}\|_\psi = 1} \|L\vec{p}\|_\psi.$$

Consistency (5.20) on the perturbed solution implies

$$\vec{\tilde{\rho}}^{\,n+1} = L\,\vec{\tilde{\rho}}^{\,n} + O\left(k(k^2+h)\right), \tag{5.23}$$

where $\vec{\tilde{\rho}}^{\,n}$ is the perturbed solution given in (5.17). Subtracting (5.23) from (5.21) yields

$$\vec{p}^{\,n+1} - \vec{\tilde{\rho}}^{\,n+1} = L\left[\vec{p}^{\,n} - \vec{\tilde{\rho}}^{\,n}\right] + O\left(k(k^2+h)\right). \tag{5.24}$$

Taking $\| \bullet \|_\psi$ norm of the both sides, using the stability, and summing over n, we have

$$\|\vec{p}^{\,n} - \vec{\tilde{\rho}}^{\,n}\|_\psi \le T \cdot O(k^2 + h), \qquad nk \le T. \tag{5.25}$$

Using the fact that $\vec{\tilde{\rho}}^{\,n} - \vec{\rho}^{\,n} = O(h)$, we obtain

$$\|\vec{p}^{\,n} - \vec{\rho}^{\,n}\|_\psi \le T \cdot O(k^2 + h). \tag{5.26}$$

Using Theorem 4.4, we see that (5.26) implies the convergence in the 2-norm:

$$\|\vec{p}^{\,n} - \vec{\rho}^{\,n}\|_2 \le e^{C_\psi} \|\vec{p}^{\,n} - \vec{\rho}^{\,n}\|_\psi \le e^{C_\psi}\, T \cdot O(k^2 + h). \tag{5.27}$$

If $k \le O(h)$, then (5.26) also implies the pointwise convergence

$$\|\vec{p}^{\,n} - \vec{\rho}^{\,n}\|_\infty \le \frac{1}{\sqrt{h}} \|\vec{p}^{\,n} - \vec{\rho}^{\,n}\|_2 \le e^{C_\psi}\, T \cdot O(\sqrt{h}). \tag{5.28}$$

6. The modified numerical method. In the consistency analysis of the previous section, we see the connection between the leading term in the local truncation error and the jump rates. Based on the lessons we learned in the consistency analysis, we will design a new set of jump rates to eliminate the first order error term caused by the discontinuity. The modified numerical method (hereafter referred to as Method 2) is as simple as Method 1. We will show that Method 2 is second order accurate even if the potential is discontinuous.

In the local truncation error in (5.20), the leading term $O(kh)$ comes from the term $v_0(t_n)$ in (5.9). At the discontinuity, if we use Method 1 defined in (3.9), then we have

$$v_0(t_n) = \left[\frac{\psi_R - \psi_L}{e^{\psi_R} - e^{\psi_L}} \left(\frac{e^{\psi_L} + e^{\psi_R}}{2} \right) - 1 \right] J(x_{l+1/2}, t_n) \neq 0.$$

This suggests a way of improving the performance of Method 1. We need to design the jump rates such that $v_0(t_n) = 0$ at the discontinuity. For that purpose, we propose Method 2:

$$\begin{aligned} F_{j+1/2} &= \frac{1}{h^2} \frac{2e^{\psi_j}}{e^{\psi_j} + e^{\psi_{j+1}}}, \\ B_{j+1/2} &= \frac{1}{h^2} \frac{2e^{\psi_{j+1}}}{e^{\psi_j} + e^{\psi_{j+1}}}. \end{aligned} \tag{6.1}$$

If we use Method 2 defined in (6.1), then we have

$$v_0(t_n) = \left[\frac{2}{e^{\psi_L} + e^{\psi_R}} \left(\frac{e^{\psi_L} + e^{\psi_R}}{2} \right) - 1 \right] J(x_{l+1/2}, t_n) = 0.$$

It can be shown that expansion (5.6) is still valid for Method 2. Consequently, expansion (5.11) is valid for Method 2 where $v_0(t_n) = 0$. Recall that for Method 1, the $O(1)$ term in (5.11) leads to an $O(h)$ error term in the numerical solution. For Method 2, $v_0(t_n) = 0$ kills the $O(1)$ term in (5.11). The third term in (5.11) is $O(h^2)$, and the remaining part of the fourth term in (5.11) is $O(h)$. Because of the special structures of vector $\{b_j\}$ in (5.13) and vector $\{a_j\}$ in (5.12), both the third term and the remaining part of the fourth term in (5.11) can be eliminated by perturbing the

exact solution by an $O(h^2)$ term. The elimination of these two terms by a perturbation of $O(h^2)$ makes Method 2 a second order method. For eliminating the third term in (5.11), we have the theorem below.

THEOREM 6.1. *Suppose $\vec{\sigma}$ is periodic, satisfies the equation*

$$h\left(F_{j-1/2}\,\sigma_{j-1} - B_{j-1/2}\,\sigma_j\right) - h\left(F_{j+1/2}\,\sigma_j - B_{j+1/2}\,\sigma_{j+1}\right) = a_j, \tag{6.2}$$

and satisfies the condition

$$\sum_{j=1}^{M} \sigma_j = 0, \tag{6.3}$$

where a_j is defined in (5.12). *Then there exists a constant C_a, independent of the numerical grid size, such that*

$$\max_j |\sigma_j| \le C_a.$$

Proof. The proof of Theorem 6.1 is similar to that of Theorem 5.1 and is skipped. ∎

Now we use the results of Theorems 5.1 and 6.1 to eliminate the third and fourth terms in (5.11). For Method 2, we consider the perturbed solution:

$$\begin{aligned} \hat{\rho}_j^n &\equiv \rho_j^n - h^2\left(v_1(t_n) + h\,\tilde{v}_2(t_n)\right) r_j - h^2\left(u(x_d^+, t_n) - u(x_d^-, t_n)\right)\sigma_j \\ &= \rho_j^n + O(h^2), \end{aligned} \tag{6.4}$$

where r_j is the solution of (5.15) and (5.16), and σ_j is the solution of (6.2) and (6.3). Theorems 5.1 and 6.1 guarantee that both r_j and σ_j are bounded by a constant, independent of the numerical grid size. The perturbed solution $\hat{\rho}_j^n$ satisfies

$$J_{j-1/2}^n\{\hat{\rho}\} - J_{j+1/2}^n\{\hat{\rho}\} = \left(J(x_{j-1/2}, t_n) - J(x_{j+1/2}, t_n)\right) + O(h^3), \tag{6.5}$$

$$\hat{\rho}_j^{n+1} - \hat{\rho}_j^n = \rho_j^{n+1} - \rho_j^n + O(kh^2). \tag{6.6}$$

Thus, the local truncation error on the perturbed solution $\hat{\rho}_j^n$ is $O\left(k(k^2+h^2)\right)$. Repeating the derivation from (5.21) to (5.28), we obtain

$$\|\vec{p}^{\,n} - \vec{\rho}^{\,n}\|_2 \le e^{C_\psi}\, T \cdot O(k^2 + h^2), \tag{6.7}$$

$$\|\vec{p}^{\,n} - \vec{\rho}^{\,n}\|_\infty \le e^{C_\psi}\, T \cdot O(h^{\frac{3}{2}}). \tag{6.8}$$

The error bound for the ∞-norm (6.8) is derived assuming the worst case scenario. As we will see in the numerical example below, the ∞-norm of the error is usually of the same order as the 2-norm of the error.

Method 2 defined in (6.1) can be viewed as constructed by using the standard finite difference on (2.1) with a special approximation for the heat conductivity:

$$e^{-\psi(x_{j+1/2})} \approx \frac{2}{e^{\psi(x_j)} + e^{\psi(x_{j+1})}}.$$

This special approximation is essential for Method 2 to achieve second order accuracy at discontinuities. Method 1 developed in [16] can be viewed as constructed by using the standard finite difference on (2.1) with approximation

$$e^{-\psi(x_{j+1/2})} \approx \frac{\psi(x_{j+1}) - \psi(x_j)}{e^{\psi(x_{j+1})} - e^{\psi(x_j)}}.$$

The numerical method previously developed by Elston and Doering in [18] can be viewed as constructed by using the standard finite difference on (2.1) with approximation

$$e^{-\psi(x_{j+1/2})} \approx e^{-\left(\frac{\psi(x_j)+\psi(x_{j+1})}{2}\right)}.$$

7. Numerical results and discussions. Now we compare the performance of three numerical methods on a model problem with discontinuous potential. For the model problem, we select the potential

$$\psi(x) = \begin{cases} 6 - 6\sin\left(\frac{\pi}{2}(x+0.5)\right), & 0 < x < 0.5, \\ 3 - 6\sin\left(\frac{\pi}{2}(x-0.5)\right), & 0.5 < x < 1. \end{cases} \tag{7.1}$$

The graph of this discontinuous potential is shown in Figure 1.1. It has a discontinuity of amplitude 3 at $x = 0.5$. We use the initial condition

$$\rho(x, 0) = 1 + \cos(2\pi x). \tag{7.2}$$

We run simulations to $t = 1$ with a wide range of values for spatial step h, and we use time step $k = h$. We compare the performance of the central difference method (3.4), Method 1 (3.9), and Method 2 (6.1). We define the error as the difference between the numerical solution obtained with a finite value of h and the converged target (the converged target is not necessarily the correct solution of the differential equation). The behavior of the error so defined tells us whether or not a method converges. However, it does not tell us whether or not the converged target is the correct solution. We estimate the error as follows. Suppose $\vec{p}^{\,n}(h)$ is the numerical solution obtained with spatial step h and time step $k = h$. The error of $\vec{p}^{\,n}(h)$ is estimated as

$$\text{error}(h) \approx C_p \left\| \vec{p}^{\,n}(h) - \vec{p}^{\,n}\left(\frac{h}{2}\right) \right\|, \tag{7.3}$$

where C_p is a constant depending on the order of the method. For methods of first order or higher, C_p is between 1 and 2. Here we simply use $C_p = 1$ (in the worst case scenario, we underestimate the error by a factor of 2). The order of a method is estimated as

$$\text{order}(h) \approx \log_2 \left(\frac{\text{error}(h)}{\text{error}\left(\frac{h}{2}\right)} \right). \tag{7.4}$$

Figure 7.1 shows the estimated errors and estimated orders for the three methods. We follow the behavior of both the 2-norm and the ∞-norm of the estimated error. Here we are solving a nondimensionalized Fokker–Planck equation. Both the time step and the spatial step are dimensionless. So $k = h$ is just a convenient choice. Strictly speaking, the error shown in Figure 7.1 is the total error in time and space estimated by comparing the numerical solution obtained using (h, k) to that of $(\frac{h}{2}, \frac{k}{2})$. However, we find that the difference in numerical solution between (h, k) and $(h, \frac{k}{2})$ is much smaller than that between (h, k) and $(\frac{h}{2}, \frac{k}{2})$ (results not shown), which indicates that the error shown in Figure 7.1 is mainly due to the spatial discretization.

For Method 1 (the second row in Figure 7.1), the estimated error decreases as $k = h$ is reduced. From the convergence analysis in the previous sections, we know that

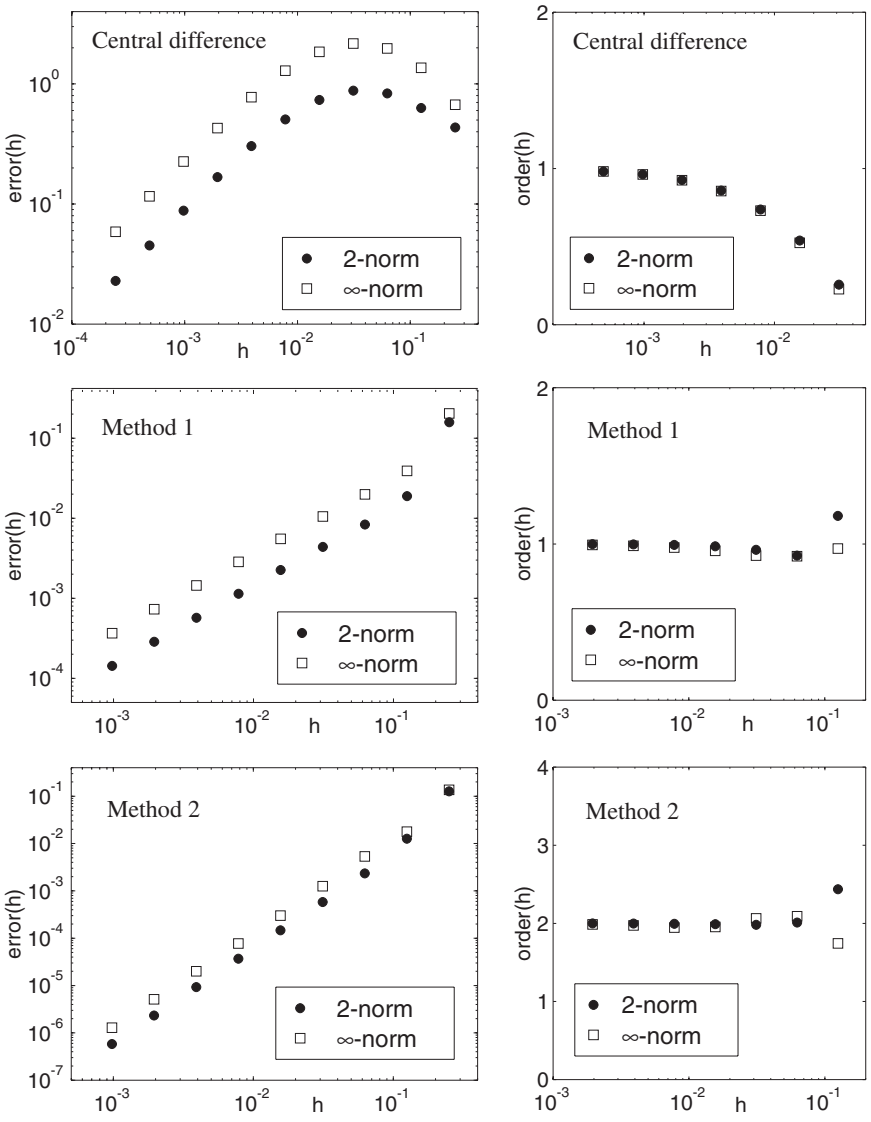

FIG. 7.1. *Estimated errors (first column) and estimated orders (second column) for the central difference method (first row), Method* 1 *(second row), and Method* 2 *(third row).*

the converged target must be the correct solution of the Fokker–Planck equation. In the presence of a discontinuity, the estimated order of accuracy of Method 1 developed in [16] is 1 for both the 2-norm and the ∞-norm. This result is consistent with the error bounds (5.27) and (5.28) derived in the previous sections. Notice that the 2-norm and the ∞-norm of the estimated error are of the same order. This tells us that although the first order error is caused by the discontinuity, it is spread to the whole region by diffusion.

For Method 2 (the third row in Figure 7.1), the estimated error decreases more rapidly as $k = h$ is reduced. The convergence analysis in the previous sections guarantees that Method 2 converges to the correct solution of the Fokker–Planck equation.

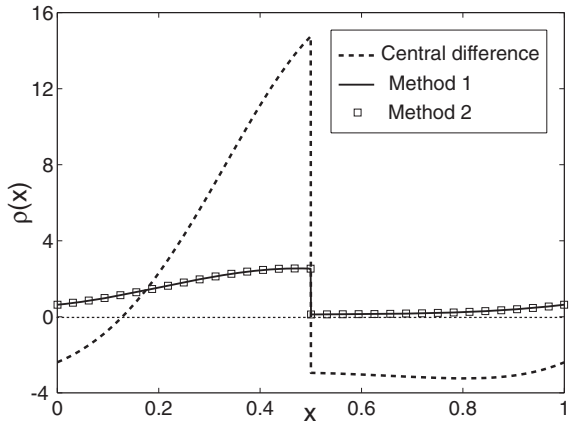

FIG. 7.2. *Numerical probability densities at $t = 1$ obtained with spatial and time steps $h = k = \frac{1}{4096}$ using, respectively, the central difference method, Method* 1*, and Method* 2*.*

Even in the presence of a discontinuity, the estimated order of accuracy for Method 2 is 2 for both the 2-norm and the ∞-norm. This result is consistent with the error bounds (6.7) and (6.8) derived in the previous section.

For the central difference method (the first row in Figure 7.1), it appears that the estimated error converges to zero as $k = h$ goes to zero. The convergence to the target is very slow. Even with $k = h = \frac{1}{4096}$, both the 2-norm and the ∞-norm of the error are still above 10^{-2}. But this is not the only defect of the central difference method. The fatal defect of the central difference method is that it converges to a wrong solution that does not satisfies condition (2.4) at the discontinuity. Figure 7.2 shows the numerical probability densities at $t = 1$ for the three methods. Notice that the probability density obtained using the central difference method is *negative* for $x > 0.5$. This is definitely wrong because the probability can never be negative. This defect of the central difference method is caused by the fact that the jump rates (3.4) may be negative at the discontinuity. Suppose the discontinuity is at $x_{l+1/2}$. The numerical probability flux at $x_{l+1/2}$ is

$$\begin{aligned} J_{l+1/2} &= h\left(F_{l+1/2}\, p_l - B_{l+1/2}\, p_{l+1}\right) \\ &= h\, B_{l+1/2}\, p_l \left[\frac{F_{l+1/2}}{B_{l+1/2}} - \frac{p_{l+1}}{p_l}\right]. \end{aligned} \tag{7.5}$$

A necessary condition for converging to the correct solution is

$$\begin{aligned} &\lim_{h\to 0} p_l = \rho(x_d^-, t), \\ &\lim_{h\to 0} p_{l+1} = \rho(x_d^+, t), \\ &\lim_{h\to 0} J_{l+1/2} = \text{finite}. \end{aligned}$$

Applying condition (2.4) yields

$$\lim_{h\to 0} \frac{p_{l+1}}{p_l} = \frac{\rho(x_d^+, t)}{\rho(x_d^-, t)} = e^{\psi(x_d^-) - \psi(x_d^+)}.$$

Multiplying (7.5) by h, using $h^2 B_{l+1/2} = O(1)$, and taking the limit as $h \to 0$, we obtain

$$\lim_{h\to 0} \frac{F_{l+1/2}}{B_{l+1/2}} = e^{\psi(x_d^-)-\psi(x_d^+)},$$

which reduces to detailed balance (3.10). Therefore, in the presence of discontinuities, detailed balance is a necessary condition for converging to the correct solution of the differential equation. Both Method 1 developed in [16] and Method 2 proposed in this paper satisfy detailed balance. The central difference method does not. For the model problem (7.1), we have

$$e^{\psi(x_d^-)-\psi(x_d^+)} = e^{-3},$$
$$\lim_{h\to 0} \frac{F^{(CD)}_{l+1/2}}{B^{(CD)}_{l+1/2}} = \frac{1 - \frac{\psi(x_d^+)-\psi(x_d^-)}{2}}{1 + \frac{\psi(x_d^+)-\psi(x_d^-)}{2}} = \frac{-1}{5} < 0.$$

The negative value of $\frac{F_{l+1/2}}{B_{l+1/2}}$ will force the ratio $\frac{p_{l+1}}{p_l}$ to be negative, which leads to negative probability in the numerical solution of the central difference method.

In conclusion, we have proved that Method 1 developed in [16] is stable and is consistent with the Fokker–Planck equation. Method 1 converges to the correct solution of the Fokker–Planck equation, and the 2-norm of the error behaves like $O(k^2 + h)$ when the potential is discontinuous. Numerical results indicate that the ∞-norm of the error is of the same order. Based on the consistency analysis, we proposed a modified version of Method 1 to eliminate the first order error caused by the discontinuity. The modified numerical method (Method 2) is guaranteed to converge to the correct solution, and the 2-norm of the error behaves like $O(k^2 + h^2)$ even in the presence of discontinuities. Again, numerical results indicate that the ∞-norm of the error is of the same order.

In stochastic ratchets with discontinuous force [20], also known as sharp stochastic ratchets [21], the potential is continuous, but the derivative of the potential is discontinuous. Originally in [20] and subsequently in [21], the transport in stochastic ratchets was studied where a particle is driven by a continuous piecewise linear potential, the Brownian noise (white noise), and an additional colored noise. They derived analytic expressions for the steady state particle current for various asymptotic limits. Now we look at the convergence of numerical methods in the case of sharp stochastic ratchets. When the potential is continuous and piecewise smooth, both Method 1 and Method 2 (the modified numerical method) converge, and the error behaves like $O(k^2 + h^2)$. This can be seen by going back to section 5. In the local truncation error in (5.20), the leading term $O(kh)$ comes from the term $v_0(t_n)$ in (5.9). $v_0(t_n)$ is nonzero only at discontinuities. For Method 1, $v_0(t_n)$ is given in (5.10). At a discontinuity on the derivative of a continuous function, we have $\psi_L = \psi_R$ and consequently $v_0(t_n) = 0$. Thus, Method 1 is second order when the potential is continuous. Method 2 (the modified numerical method) is already second order even when the potential is discontinuous.

All of the conclusions above for Method 1 are also true for the numerical method previously developed by Elston and Doering [18]. More specifically, the numerical stability proved in section 4 depends on two main features of the numerical method, (i) all jump rates being positive and (ii) detailed balance being preserved, which are satisfied in the method of [18]. The numerical consistence away from the discontinuities is obtained by doing Taylor expansion. The key feature we utilized in section 5

to derive the numerical consistence at the discontinuities is again detailed balance. Therefore, all the analysis in sections 4 and 5 for Method 1 can be extended to the method in [18].

In the numerical simulations above, we also examined the behavior of the central difference method. We found that in the presence of discontinuities, the central difference method converges to a wrong solution that does not satisfy condition (2.4). We showed that in the presence of discontinuities, detailed balance is a necessary condition for converging to the correct solution. Both Method 1 and Method 2 satisfy detailed balance. The central difference method does not, which explains the fatal defect of the central difference method.

Appendix A. In this appendix, we derive (5.6). We start by expanding function $\frac{x}{e^x-1}$ around $x=0$:

$$\frac{x}{e^x-1} = 1 - \frac{1}{2}x + \frac{1}{12}x^2 + 0 \times x^3 + O\left(x^4\right). \tag{A.1}$$

Using (A.1) to expand jump rates $F_{j+1/2}$ and $B_{j+1/2}$ in terms of $\delta\psi_{j+1/2}$, we get

$$\begin{aligned} F_{j+1/2} &= \frac{1}{h^2}\frac{\delta\psi_{j+1/2}}{e^{\delta\psi_{j+1/2}}-1} \\ &= \frac{1}{h^2}\left[1 - \frac{1}{2}\delta\psi_{j+1/2} + \frac{1}{12}(\delta\psi_{j+1/2})^2 + O\left((\delta\psi_{j+1/2})^4\right)\right], \end{aligned} \tag{A.2}$$

$$\begin{aligned} B_{j+1/2} &= \frac{1}{h^2}\frac{\delta\psi_{j+1/2}\, e^{\delta\psi_{j+1/2}}}{e^{\delta\psi_{j+1/2}}-1} \\ &= \frac{1}{h^2}\frac{(-\delta\psi_{j+1/2})}{e^{-\delta\psi_{j+1/2}}-1} \\ &= \frac{1}{h^2}\left[1 + \frac{1}{2}\delta\psi_{j+1/2} + \frac{1}{12}(\delta\psi_{j+1/2})^2 + O\left((\delta\psi_{j+1/2})^4\right)\right]. \end{aligned} \tag{A.3}$$

Substituting $F_{j+1/2}$, $B_{j+1/2}$, ρ_j^n, and ρ_{j+1}^n into (5.2) yields

$$\begin{aligned} J_{j+1/2}^n &= h\left(F_{j+1/2}\,\rho_j^n - B_{j+1/2}\,\rho_{j+1}^n\right) \\ &= \frac{1}{h}\left[\left(\rho_j^n - \rho_{j+1}^n\right) - \frac{1}{2}\delta\psi_{j+1/2}\left(\rho_j^n + \rho_{j+1}^n\right)\right. \\ &\qquad \left. + \frac{1}{12}(\delta\psi_{j+1/2})^2\left(\rho_j^n - \rho_{j+1}^n\right) + O\left((\delta\psi_{j+1/2})^4\right)\right]. \end{aligned} \tag{A.4}$$

Expanding $\delta\psi_{j+1/2}$, ρ_j^n, and ρ_{j+1}^n around $x = x_{j+1/2}$, we have

$$\delta\psi_{j+1/2} = h\,\psi'_{j+1/2} + \frac{h^3}{24}\psi'''_{j+1/2} + O\left(h^5\right),$$

$$\rho_j^n - \rho_{j+1}^n = -h\left(\frac{\partial\rho}{\partial x}\right)_{j+1/2}^n - \frac{h^3}{24}\left(\frac{\partial^3\rho}{\partial x^3}\right)_{j+1/2}^n + O\left(h^5\right),$$

$$\rho_j^n + \rho_{j+1}^n = 2\left(\rho(x,t)\right)_{j+1/2}^n + \frac{h^2}{4}\left(\frac{\partial^2\rho}{\partial x^2}\right)_{j+1/2}^n + O\left(h^4\right).$$

Here we used the shorthand notation $(g(x,t))_j^n = g(x_j, t_n)$. Substituting these expansions into (A.4), we obtain the expansion for the probability flux

$$J_{j+1/2}^n = -\left(\psi'\rho + \frac{\partial \rho}{\partial x}\right)_{j+1/2}^n - h^2\left(\frac{1}{24}\frac{\partial^3 \rho}{\partial x^3} + \frac{1}{8}\psi'\frac{\partial^2 \rho}{\partial x^2} + \frac{1}{12}(\psi')^2\frac{\partial \rho}{\partial x} + \frac{1}{24}\psi'''\rho\right)_{j+1/2}^n + O\left(h^3\right),$$

which corresponds to (5.6).

Appendix B. In this appendix, we prove Theorem 5.1. We first rewrite the numerical probability flux as

$$\begin{aligned} J_{j+1/2} &= h\left(F_{j+1/2}\, r_j - B_{j+1/2}\, r_{j+1}\right) \\ &= \frac{1}{h}\,\frac{\psi_{j+1}-\psi_j}{e^{\psi_{j+1}}-e^{\psi_j}} e^{\psi_j}\, r_j - \frac{1}{h}\,\frac{\psi_{j+1}-\psi_j}{e^{\psi_{j+1}}-e^{\psi_j}} e^{\psi_{j+1}}\, r_{j+1} \\ &= \frac{1}{h}\,\frac{\psi_{j+1}-\psi_j}{e^{\psi_{j+1}}-e^{\psi_j}}\left(e^{\psi_j}\, r_j - e^{\psi_{j+1}}\, r_{j+1}\right). \end{aligned} \tag{B.1}$$

Suppose r_j is the solution of (5.15) and (5.16). Let $\tilde{r}_j = e^{\psi_j}\, r_j$. $\tilde{r}_j$ satisfies the equation

$$\frac{1}{h}\,\frac{\psi_j-\psi_{j-1}}{e^{\psi_j}-e^{\psi_{j-1}}}\left(\tilde{r}_{j-1}-\tilde{r}_j\right) - \frac{1}{h}\,\frac{\psi_{j+1}-\psi_j}{e^{\psi_{j+1}}-e^{\psi_j}}\left(\tilde{r}_j-\tilde{r}_{j+1}\right) = b_j \tag{B.2}$$

and the condition

$$\sum_{j=1}^{M} e^{-\psi_j}\,\tilde{r}_j = 0. \tag{B.3}$$

We construct $\tilde{r}_j$ starting at $j = l+1$ with

$$\tilde{r}_{l+1} = -c_1 \quad \text{and} \quad \frac{1}{h}\,\frac{\psi_{l+2}-\psi_{l+1}}{e^{\psi_{l+2}}-e^{\psi_{l+1}}}\left(\tilde{r}_{l+1}-\tilde{r}_{l+2}\right) = -c_2,$$

where c_1 and c_2 are two coefficients to be determined. Because b_j, as defined in (5.13), satisfies $b_j = 0$ for $j = l+2, \ldots, M+l-1$, we immediately obtain that

$$\frac{1}{h}\,\frac{\psi_{j+1}-\psi_j}{e^{\psi_{j+1}}-e^{\psi_j}}\left(\tilde{r}_j-\tilde{r}_{j+1}\right) = -c_2 \quad \text{for } j = l+2, \ldots, M+l-1.$$

This allows us to write $\tilde{r}_{j+1}$ in terms of $\tilde{r}_j$:

$$\tilde{r}_{j+1} = \tilde{r}_j + c_2\left(h\frac{e^{\psi_{j+1}}-e^{\psi_j}}{\psi_{j+1}-\psi_j}\right).$$

Summing over j, we get

$$\tilde{r}_i = -c_1 + c_2\sum_{j=l+1}^{i-1}\left(h\frac{e^{\psi_{j+1}}-e^{\psi_j}}{\psi_{j+1}-\psi_j}\right) \quad \text{for } i = l+2, \ldots, M+l. \tag{B.4}$$

For $\tilde{r}_j$ to solve (B.2), it needs to satisfy

$$\frac{1}{h}\,\frac{\psi_{l+1}-\psi_l}{e^{\psi_{l+1}}-e^{\psi_l}}\left(\tilde{r}_l-\tilde{r}_{l+1}\right) = \frac{1}{h} - c_2. \tag{B.5}$$

Using the fact that $\tilde{r}_j$ is periodic and substituting (B.4) into (B.5) yields an equation for c_2:

$$c_2 \frac{\psi_{l+1} - \psi_l}{e^{\psi_{l+1}} - e^{\psi_l}} \sum_{j=l+1}^{M+l-1} \left(h \frac{e^{\psi_{j+1}} - e^{\psi_j}}{\psi_{j+1} - \psi_j} \right) = 1 - c_2 h. \tag{B.6}$$

It follows that

$$c_2 = \left[h + \frac{\psi_{l+1} - \psi_l}{e^{\psi_{l+1}} - e^{\psi_l}} \sum_{j=l+1}^{M+l-1} \left(h \frac{e^{\psi_{j+1}} - e^{\psi_j}}{\psi_{j+1} - \psi_j} \right) \right]^{-1}. \tag{B.7}$$

The sum in (B.7) is approximately an integral

$$\sum_{j=l+1}^{M+l-1} \left(h \frac{e^{\psi_{j+1}} - e^{\psi_j}}{\psi_{j+1} - \psi_j} \right) = \int_0^1 e^{\psi(x)} dx + O(h).$$

Substituting this result into (B.7), we have

$$c_2 = \frac{e^{\psi_R} - e^{\psi_L}}{\psi_R - \psi_L} \left[\int_0^1 e^{\psi(x)} dx \right]^{-1} + O(h). \tag{B.8}$$

Thus, for h small enough, c_2 is positive and bounded.

c_1 is determined by condition (B.3). Notice that $\tilde{r}_j$, as given in (B.4), is monotonically increasing for $j = l+1, \ldots, M+l$. If $c_1 = 0$, then we have $\tilde{r}_{l+1} = 0$ and $\tilde{r}_j > 0$ for $j = l+2, \ldots, M+l$. Consequently, we have $\sum_{j=1}^{M} e^{-\psi_j} \tilde{r}_j > 0$. Now we select c_1 to make $\tilde{r}_{M+l} = 0$:

$$\hat{c}_1 = c_2 \sum_{j=l+1}^{M+l-1} \left(h \frac{e^{\psi_{j+1}} - e^{\psi_j}}{\psi_{j+1} - \psi_j} \right) = \frac{e^{\psi_R} - e^{\psi_L}}{\psi_R - \psi_L} + O(h).$$

In this case, we have $\tilde{r}_{M+l} = 0$ and $\tilde{r}_j < 0$ for $j = l+1, \ldots, M+l-1$. Consequently, we have $\sum_{j=1}^{M} e^{-\psi_j} \tilde{r}_j < 0$. The value of c_1 that satisfies condition (B.3) is between 0 and $\hat{c}_1$. Thus, for h small enough, c_1 is positive and bounded:

$$0 < c_1 < \frac{e^{\psi_R} - e^{\psi_L}}{\psi_R - \psi_L} + O(h). \tag{B.9}$$

Substituting (B.8) and (B.9) into (B.4), we conclude that

$$\max_j |\tilde{r}_j| \leq \frac{e^{\psi_R} - e^{\psi_L}}{\psi_R - \psi_L} + O(h), \tag{B.10}$$

which leads directly to the conclusion of Theorem 5.1.

Acknowledgment. The author would like to thank anonymous referees for their constructive comments and suggestions in improving the manuscript.

REFERENCES

[1] H. C. Berg, *Random Walks in Biology*, Princeton University Press, Princeton, NJ, 1993.

[2] J. Abrahams, A. Leslie, R. Lutter, and J. Walker, *Structure at* 2.8*A resolution of F*1-*ATPase from bovine heart mitochondria*, Nature, 370 (1994), pp. 621–628.
[3] H. Noji, R. Yasuda, M. Yoshida, and K. Kinosita, *Direct observation of the rotation of F*1-*ATPase*, Nature, 386 (1997), pp. 299–302.
[4] H. Wang and G. Oster, *Energy transduction in the F*1 *motor of ATP synthase*, Nature, 396 (1998), pp. 279–282.
[5] C. Coppin, D. Pierce, L. Hsu, and R. Vale, *The load dependence of kinesin's mechanical cycle*, Proc. Nat. Acad. Sci. U.S.A., 94 (1997), pp. 8539–8544.
[6] K. Visscher, M. Schnitzer, and S. Block, *Single kinesin molecules studied with a molecular force clamp*, Nature, 400 (1999), pp. 184–189.
[7] J. Prost, J. Chauwin, L. Peliti, and A. Ajdari, *Asymmetric pumping of particles*, Phys. Rev. Lett., 72 (1994), pp. 2652–2655.
[8] R. Astumian, *Thermodynamics and kinetics of a Brownian motor*, Science, 276 (1997), pp. 917–922.
[9] T. Elston, H. Wang, and G. Oster, *Energy transduction in ATP synthase*, Nature, 391 (1998), pp. 510–514.
[10] H. Wang, *Mathematical theory of molecular motors and a new approach for uncovering motor mechanism*, IEE Proc. Nanobiotechnol., 150 (2003), pp. 127–133.
[11] F. Reif, *Fundamentals of Statistical and Thermal Physics*, McGraw–Hill, New York, 1985.
[12] H. Risken, *The Fokker-Planck Equation*, 2nd ed., Springer, Berlin, 1989.
[13] A. Einstein, *Investigation on the Theory of the Brownian Motion*, Dover, New York, 1956.
[14] C. Peskin, G. Odell, and G. Oster, *Cellular motions and thermal fluctuations: The Brownian ratchet*, Biophys. J., 65 (1993), pp. 316–324.
[15] T. C. Elston and C. S. Peskin, *The role of protein flexibility in molecular motor function: Coupled diffusion in a tilted periodic potential*, SIAM J. Appl. Math., 60 (2000), pp. 842–867.
[16] H. Wang, C. Peskin, and T. Elston, *A robust numerical algorithm for studying biomolecular transport processes*, J. Theoret. Biol., 221 (2003), pp. 491–511.
[17] R. D. Richtmyer and K. W. Morton, *Difference Methods for Initial Value Problems*, Wiley-Interscience, New York, 1967.
[18] T. Elston and C. Doering, *Numerical and analytical studies of nonequilibrium fluctuation induced transport processes*, J. Statist. Phys., 83 (1996), pp. 359–383.
[19] M. L. Juncosa and D. Young, *On the Crank-Nicolson procedure for solving parabolic partial differential equations*, Proc. Cambridge Philos. Soc., 53 (1957), pp. 448–461.
[20] C. R. Doering, L. A. Dontcheva, and M. M. Klosek, *Constructive role of noise: Fast fluctuation asymptotics of transport in stochastic ratchets*, Chaos, 8 (1998), pp. 643–649.
[21] M. M. Kłosek and R. W. Cox, *Steady-state currents in sharp stochastic ratchets*, Phys. Rev. E (3), 60 (1999), pp. 3727–3735.
[22] R. Feynman, R. Leighton, and M. Sands, *The Feynman Lectures on Physics*, Addison–Wesley, Reading, MA, 1963.
[23] G. Dal Maso, Ph. Le Floch, and F. Murat, *Definition and weak stability of non-conservative products*, J. Math. Pures Appl. (9), 74 (1995), pp. 483–548.
[24] E. Godlewski and P. A. Raviart, *Numerical Approximation of Hyperbolic Systems of Conservation Laws*, Appl. Math. Sci. 118, Springer, New York, 1996.